Supporting Information

Chemical etching induced microporous nickel backbones decorated with metallic Fe@ hydroxide nanocatalysts: An efficient and sustainable OER anode toward industrial alkaline water splitting

Nabeen K. Shrestha*[a], Supriya A. Patil[b], Jonghoon Han[a], Sangeun Cho[a], Akbar I. Inamdar[a], Hyungsang Kim*[a], Hyunsik Im*[a]

[a]Division of Physics and Semiconductor Science, Dongguk University, Seoul 04620, South Korea.

[b]Department Nanotechnology & Advanced Materials Engineering, Sejong University, Seoul 05006, South Korea.

**Corresponding authors*: nabeenkshrestha@hotmail.com, hskim@dongguk.edu, hyunsik7@dongguk.edu

SI-1:

The standard reduction electrode potential $E_{Fe3+/Fe0}$ is calculated as follows.

$Fe^{2+} + 2e^{-} \rightarrow Fe$ ……………….(1), $E_1^0 = -0.44$ V

$Fe^{3+} + e^{-} \rightarrow Fe^{2+}$……………….(2), $E_2^0 = 0.77$ V

(E_1^0 and E_2^0 values were taken from the electrochemical series)

Adding equation (1) *and* (2)

$Fe^{3+} + 3e^{-} \rightarrow Fe$………………..(3), $\mathbf{E_3^0}$

Let, ΔG_1, ΔG_2 and ΔG_3 are the free energies of the reaction (1), (2) and (3).

Then, $\Delta G_1 + \Delta G_2 = \Delta G_3$………(4)

Here, $\Delta G = -nE^0F$ ……………(5), where n = number of electron involved in the electrode reaction, E^0= standard electrode potential in volt, and F = Faraday constant.

Hence, from (1), (2), (4) and (5):

$-2 \times F \times (-0.44) + 1 \times F \times 0.77 = -3 \times F \times E_3^0$

As a result: $\mathbf{E^0_{Fe3+/Fe} = E_3^0 = +0.037}$ **V**.

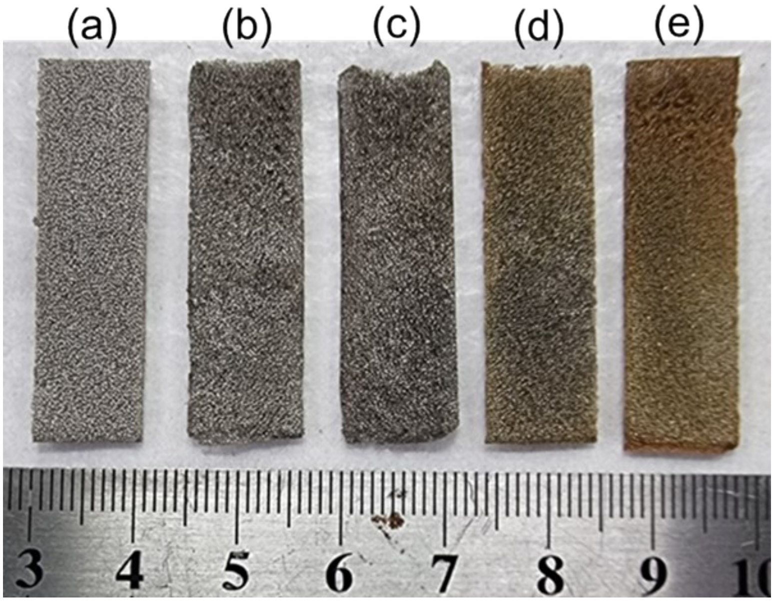

Figure 1. Images of Ni foam (a) before and after immersion of the foam in an ethanolic $FeCl_3$ solution at 50 °C for (b) 6 h, (c) 12 h, (d) 18 h, and (e) 24 h.

.

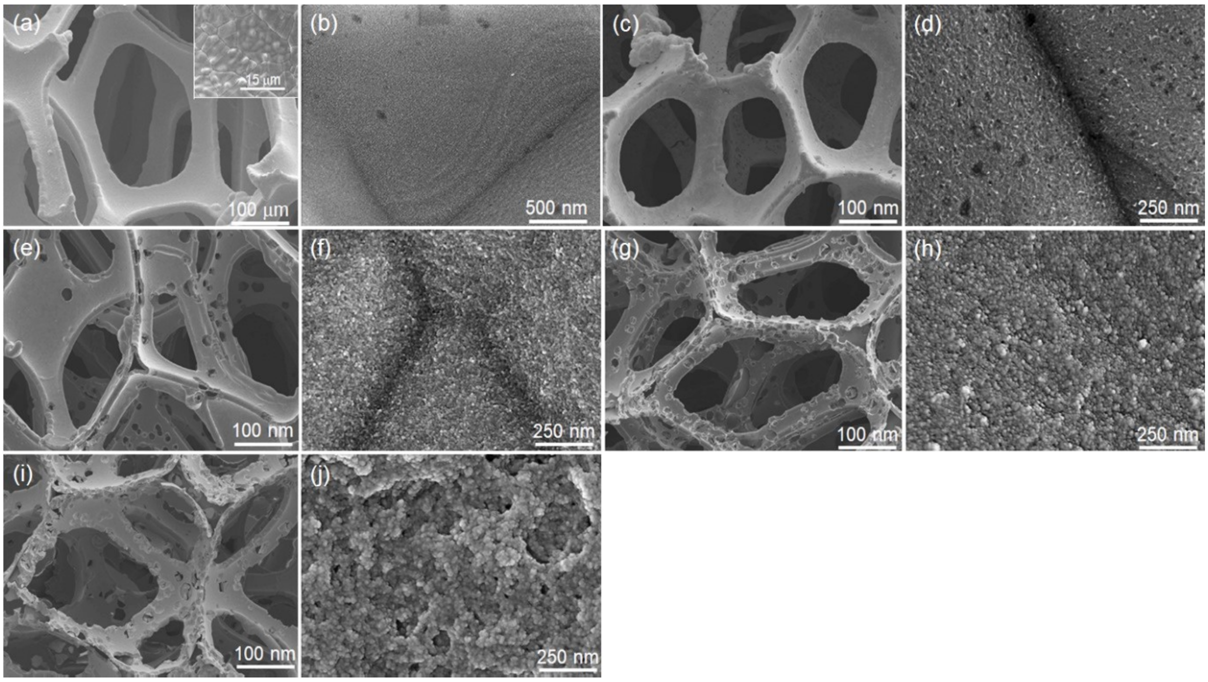

Figure S2. SEM images showing a surface view of (a) pristine NF, (b) pristine NF under high magnification, and NF in an ethanolic $FeCl_3$ solution at 50 ºC for (c) 6 h (Fe-6h/NF) under (d) high magnification, (e) 12 h (Fe-12h/NF) under (f) high magnification, (g) 18 h (Fe-18h/NF) under (h) high magnification, and (i) 24 h (Fe-24h/NF) under (j) high magnification. The inset image in (a) presents the NF under high magnification showing the crystal grain boundaries.

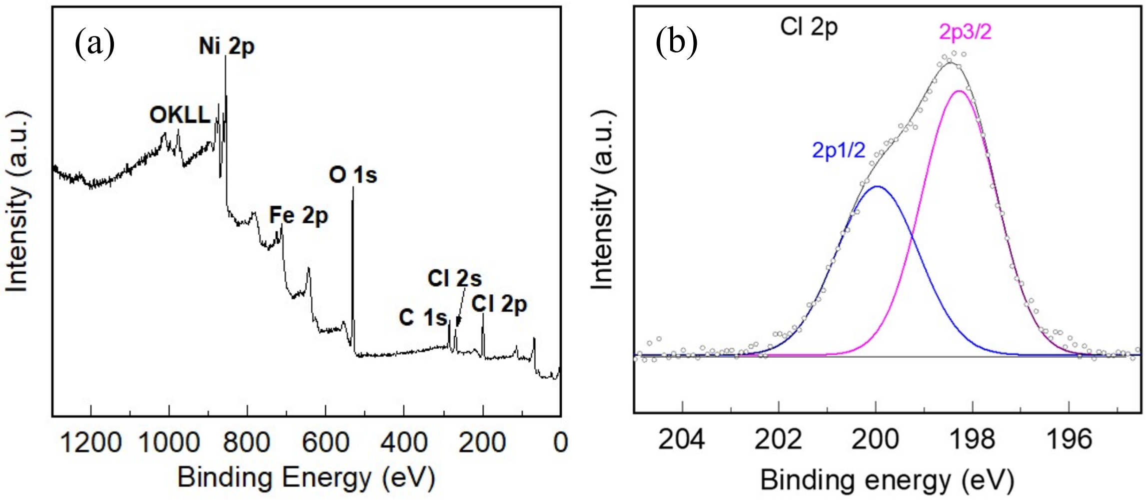

Figure S3. (a) XPS survey spectrum of etched NF (Fe-18h/NF) in ethanolic $FeCl_3$ at 50 ºC, and (b) Cl 2p spectrum of the same sample.

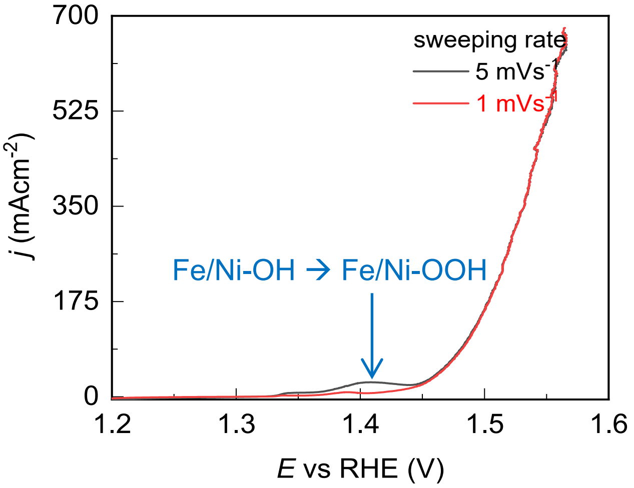

Figure S4. *iR* compensated linear sweep voltammograms of the etched NF (Fe-18h/NF) in 1 M KOH solution.

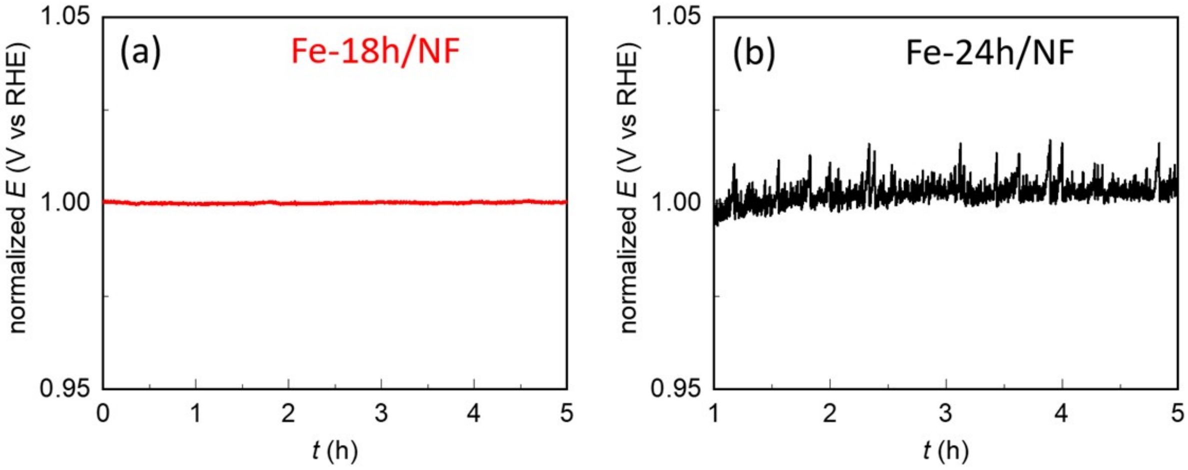

Figure S5. Normalized chronopotentiometric curves obtained at an applied current density of 350 mAcm^{-2} in a 1 M KOH aqueous electrolyte from (a) Fe-18h/NF and (b) Fe-24h/NF electrodes.

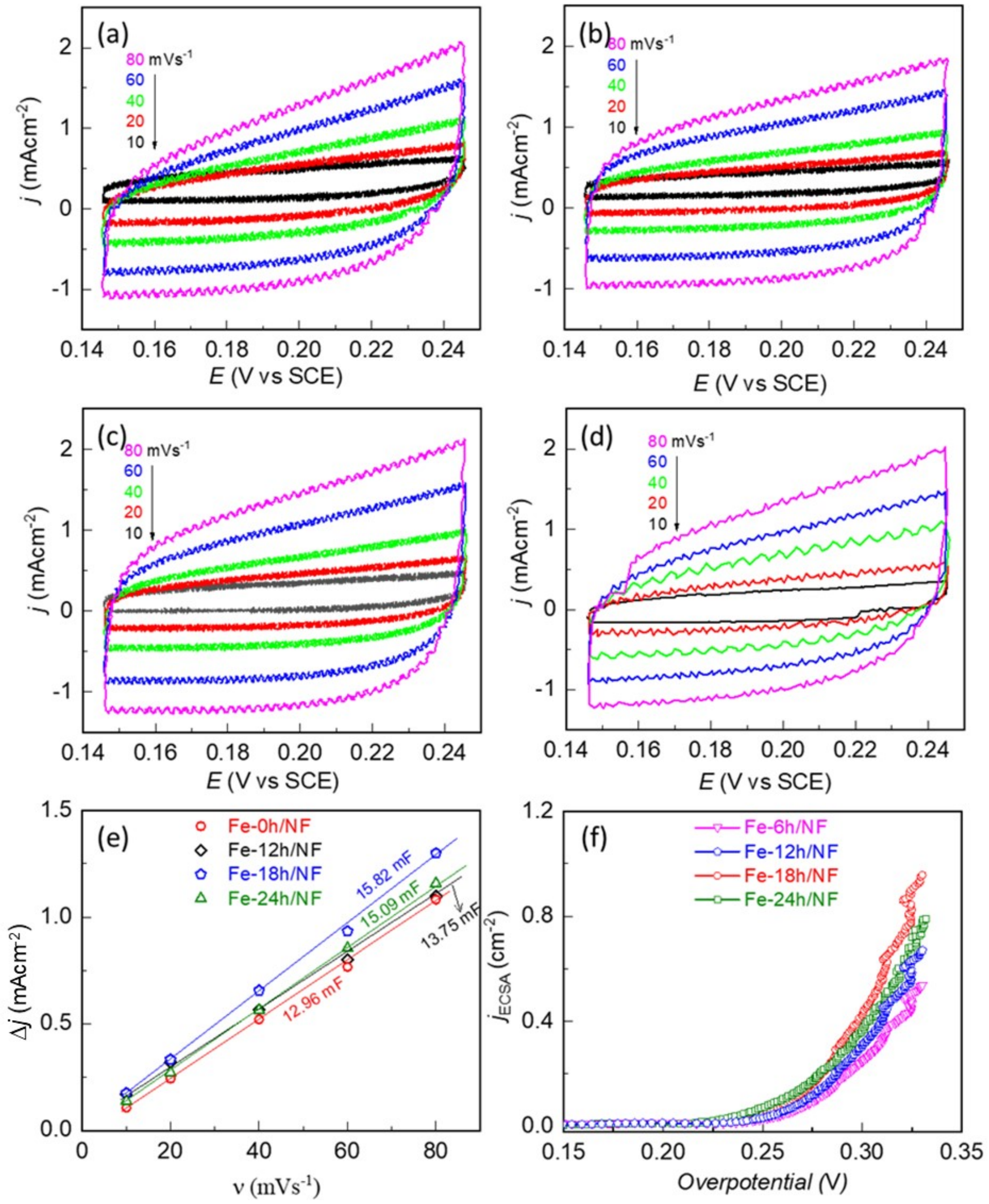

(g)

	Fe-6h/NF	Fe-12h/NF	Fe-18h/NF	Fe-24h/NF
ECSA (cm^2)	589.09	625.00	719.09	685.90

Figure S6. Cyclic voltammograms (CVs) of etched NF at various scan rates in a 1 M KOH solution: (a) Fe-6h/NF, (b) Fe-12h/NF, (c) Fe-18h/NF, and (d) Fe-24h/NF. (e) Average current density ($\Delta j = (j_a - j_c)/2$) against the scan rate showing the double-layer capacitance (C_{dl}) extracted from the corresponding CVs. (f) *iR* compensated LSVs based on the ECSA-specific current density in a 1M KOH solution. (g) Table showing the electrochemically active surface area (ECSA) in cm^2.

The double layer capacitance (C_{dl}) was determined from a CV using the equation: $C_{dl} = \Delta j\ (j_a - j_c)/2\nu$, where j_a and j_c are anodic and cathodic current densities at $\Delta E = 0.2$ V and ν is the scan rate in mVs^{-1}. The non-Faradic current density based electrochemically active surface area (ECSA) was estimated according to the equation: ECSA = C_{dl}/C_s, where C_s is the specific capacitance of the electrode and was taken as 0.022 mFcm^{-2} in 1 M KOH electrolyte.[1] ECSA, thus, estimated are tabulated in Fig. "(g)".

[1] *J. Am. Chem. Soc*. 2013, 135, 45, 16977.

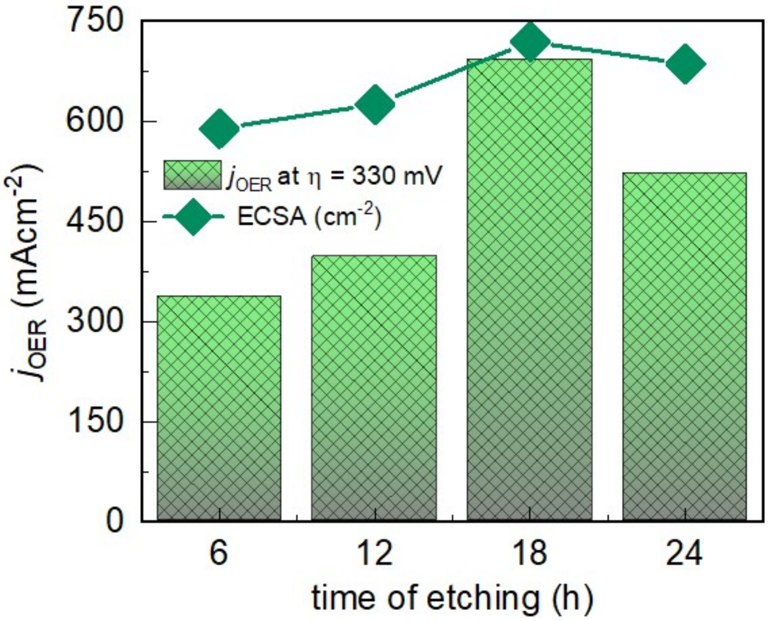

Figure S7. Electrochemically active surface area (ECSA) and OER current density (j_{OER}) exhibited by the nickel foam etched for 6, 12, 18 and 24 h in ethanolic $FeCl_3$ solution at 50 °C.

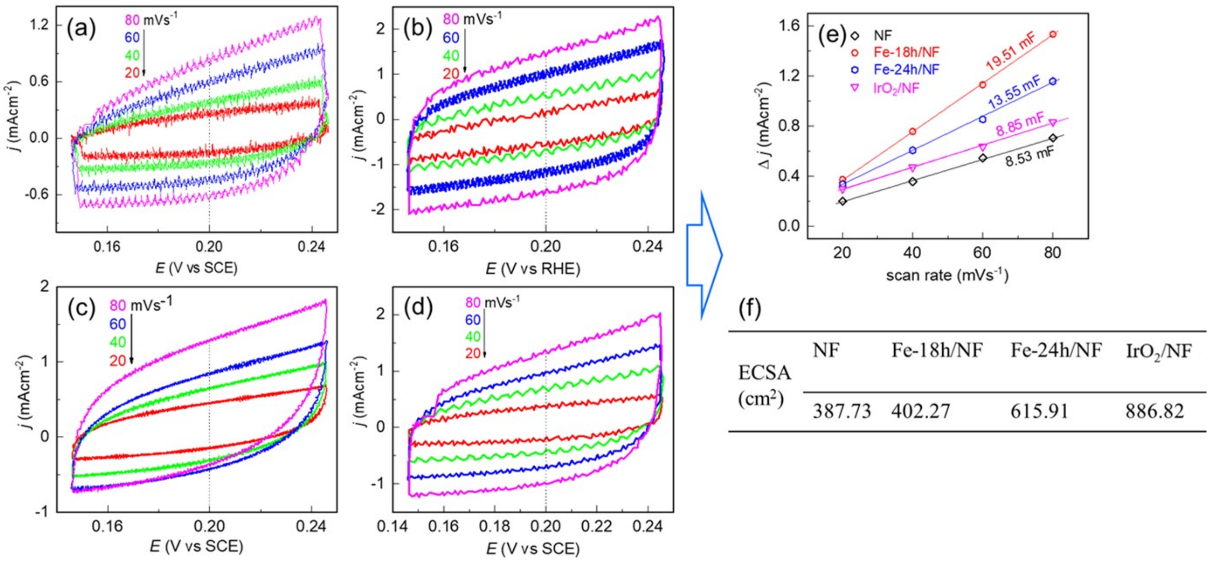

	NF	Fe-18h/NF	Fe-24h/NF	IrO_2/NF
ECSA (cm^2)	387.73	402.27	615.91	886.82

Figure S8. CV curves recorded in the non-Faradic regions of (a) NF, (b) Fe-18h/NF, (c) Fe-24h/NF, and (d) IrO_2/NF, in a 1 M KOH solution at various scan rates (20 to 80 mV s^{-1}). (e) Average non-Faradaic current density ($\Delta j = (j_a\text{-}j_c)/2$) obtained from CV curves at 0.20 V as a function of the scan rate, and (f) a comparison with the ECSA.

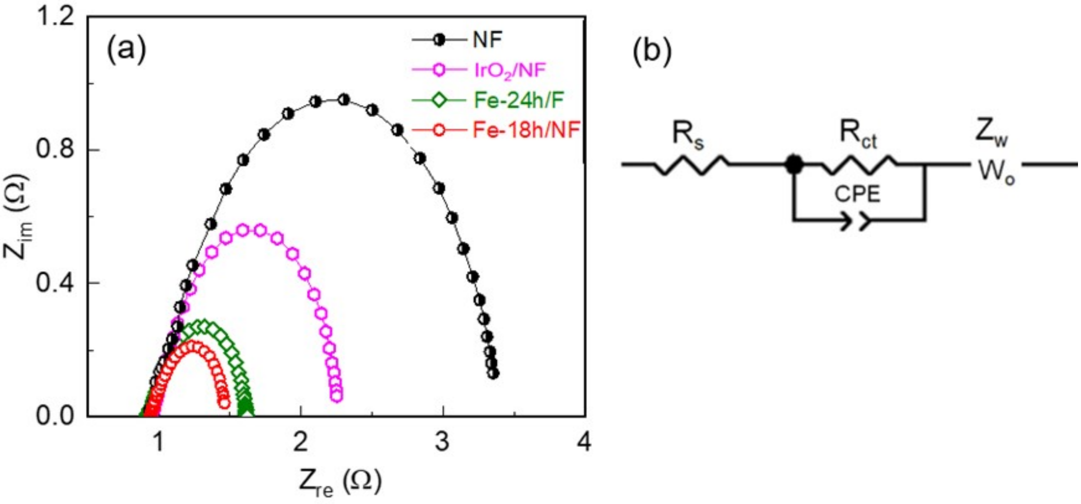

(c)

	NF	Fe-18h/NF	Fe-24h/NF	IrO_2/NF
R_s (Ω)	0.93	0.93	0.92	0.94
R_{ct} (Ω)	3.36	1.45	1.62	2.24

Figure S9. (a) Nyquist plot derived from the electrochemical impedance spectra, (b) the equivalent circuit employed to fit the impedance data, and (c) the table showing the series resistance (R_s) and charge transfer resistance (R_{ct}) extracted from the Nyquist plot.

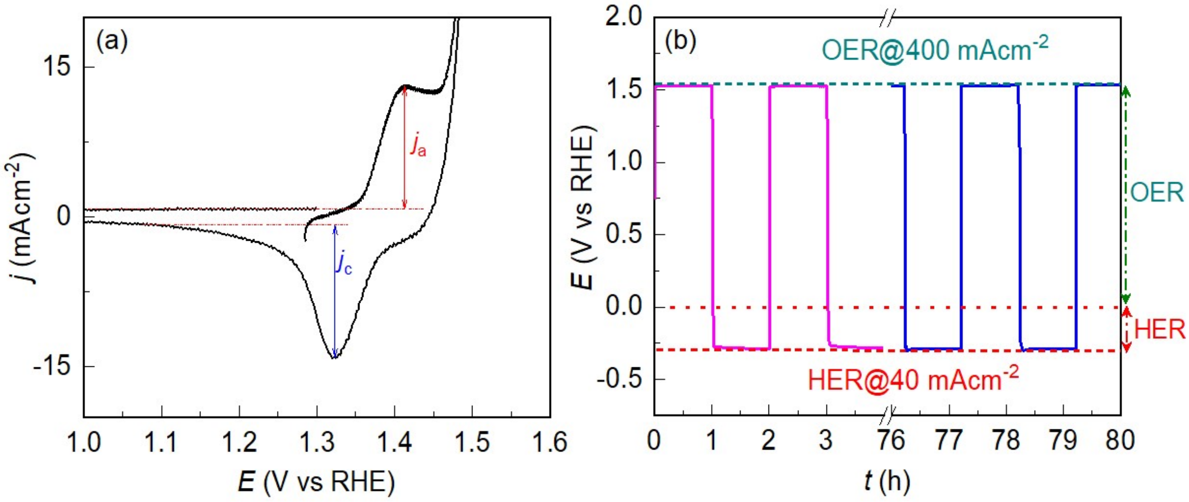

Figure S10. (a) CV of the Fe-18h/NF electrode in a 1 M KOH solution at a scan rate of 5 mVs^{-1} showing a pair of reversible redox peaks for M–OH ↔ M–OOH, where the current density in the anodic (j_a) and the cathodic (j_c) directions are almost equal. (b) Chronopotentiometric response of the Fe-18h/NF electrode in a 1 M KOH solution at the beginning and end of 80 h under periodic polarization between +400 and –40 mAcm^{-2}.

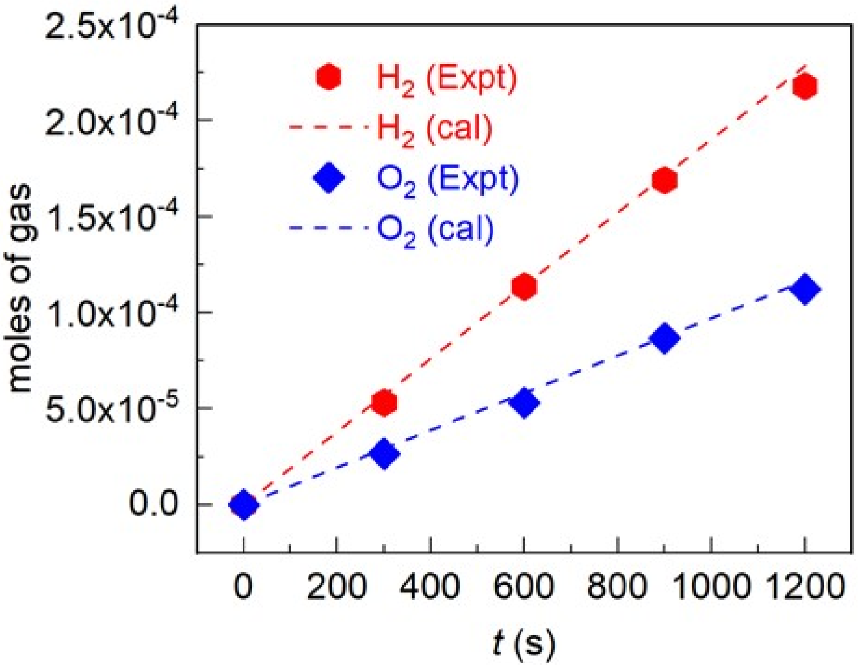

Figure S11. Faradic current efficiency for the HER and OER of the Fe-18h/NF electrode measured at 25 mAcm^{-2} in a 30% KOH aqueous electrolyte using conventional water displacement. The active electrode area of the cathode and anode was 1.5 cm^{-2}.

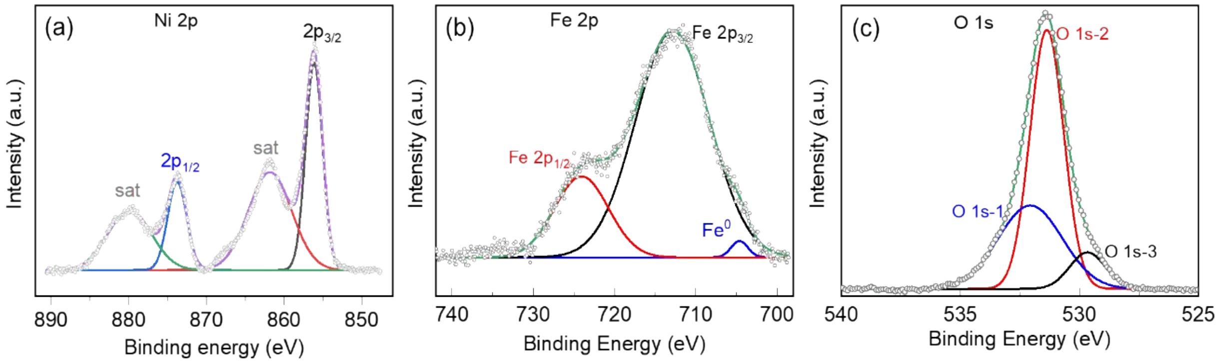

Figure 12. XPS spectra for the Fe-18h/NF electrode after stability testing for 96 h in a 30 wt% KOH solution.

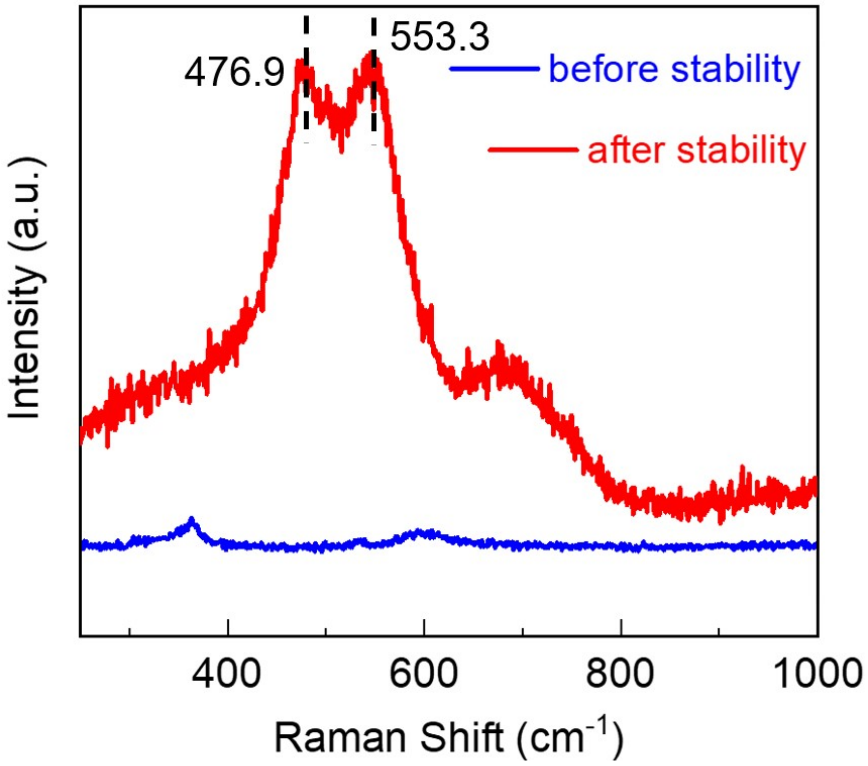

Figure. S13. Raman spectra for the Fe-18h/NF electrode before (i.e., as-synthesized) and after electrochemical stability testing. The pair of peaks observed after stability testing indicates the presence of the NiOOH-FeOOH (MOOH) phase.

.

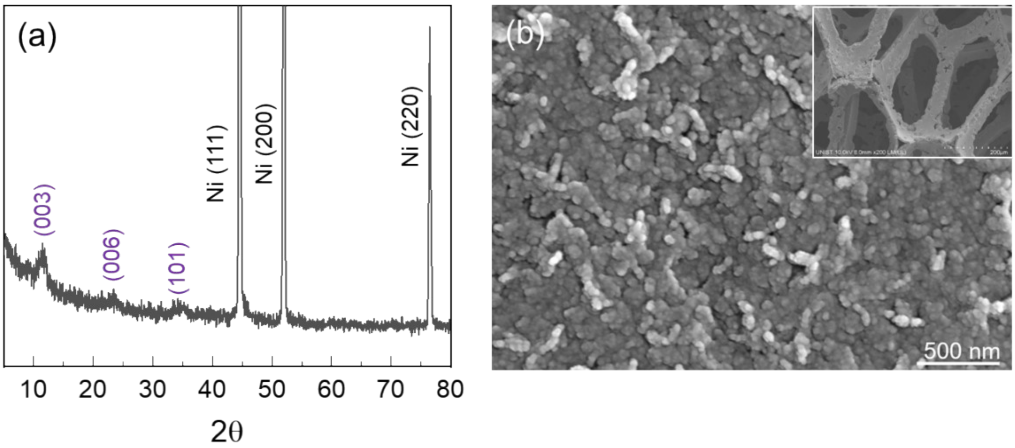

Figure. S14. XRD patterns and an SEM surface view of the Fe-18h/NF electrode after stability testing for 96 h in a 30 wt% KOH solution. Inset image in “(b)” is a low magnification of the same electrode.

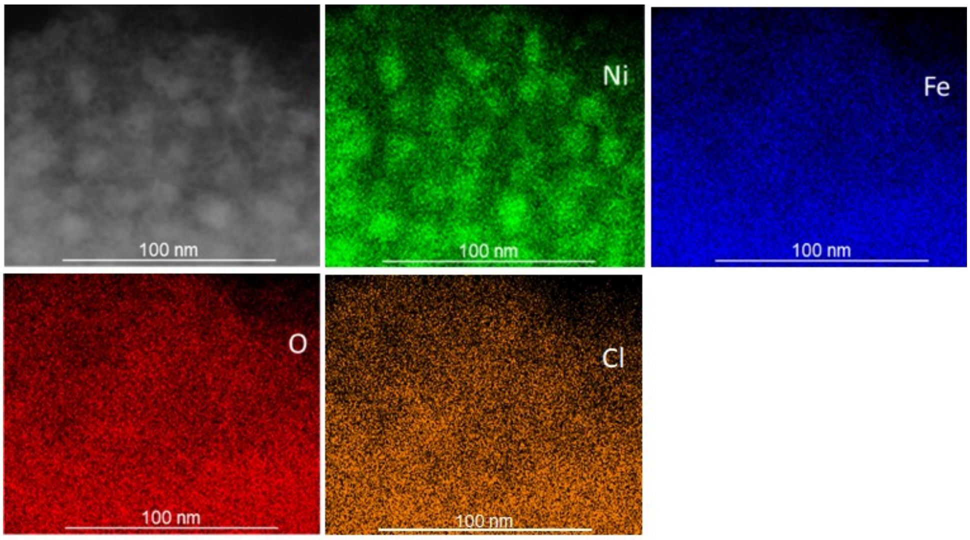

Figure S15. High-angle annular dark-field (HAADF) image and elemental mappings showing the uniform distribution of the constituent Ni, Fe, and O within the Fe-18h/NF electrode after stability testing for 96 h in a 30 wt% KOH solution.

Table S1. Comparison of OER performance for Fe-18h/NF and Fe-24h/NF with those of state-of-the art electrocatalysts under alkaline conditions.

	Anode materials	Electrolyte	*j* (mAcm^{-2})	Overpotential (mV)	Tafel slope (mVdec^{-1})	Ref
1	Fe-18h/NF	1 M KOH	10	220	47.3	**This work**
			50	247		
			100	270		
			250	290		
			500	310		
	Fe-24h/NF		10	215		
			50	245		
			100	270		
			250	300		
			500	330		
	IrO_2 /NF		10	260		
			50	310		
			100	330		
			250	380		

			375	390		
2	5h-A-NF		500	346	62.2	[1]
3	0.14 M Fe/A-NF		50 500	244 334	69.6	[2]
4	NiO/NiNDs@NF		50	360	90.0	[3]
5	Inverse-NP		10 50	300 362	90.0	[4]
6	Ni-CLPs0°,activated		10 100	204 300	-	[5]
7	NFN-MOF/NF		10 250 500	240 335 360	58.8	[6]
8	NiFe/NiCo$_2$O$_4$/NF		10 500	240 310	38.8	[7]
9	MFN-MOFs(2:1)/NF		50 500	235 294	55.4	[8]
10	Ni-QDs@NC@rGO		10	265	65.0	[9]
11	Fe-O-Ni(OH)$_2$/NF		10 100 500	185 220 261		[10]
12	NiFeOx/NF		100	260	28.0	[11]
13	Ni-Fe NP/CFP		10 20 100	210 230 270	-	[12]
14	NiFe-LDH/Mxene/NF		10 500	229 300	44.0	[13]
15	Hier-NiFe@sCNTs		30 100 500	209 279 321	65.7	[14]
16	so-Fe-Ni(OH)$_2$ TTAs		10	226	35.9	[15]
17	Ru-NiFe-P		50 100	227 242	66.1	[16]

SI-References

[1] Y.J. Son, K. Kawashima, B.R. Wygant, C.H. Lam, J.N. Burrow, H. Celio, A. Dolocan, J.G. Ekerdt, C.B. Mullins, *ACS Nano*. **2021**, *15*, 3468.

[2] X.F. Chuah, C.T. Hsieh, C.L. Huang, D. Senthil Raja, H.W. Lin, S.Y. Lu, *ACS Appl. Energy Mater*. **2019**, *2*, 743.

[3] H. Yu, T. Quan, S. Mei, Z. Kochovski, W. Huang, H. Meng, Y. Lu, *Nano-Micro Lett*. **2019**, *11*, 41.

[4] R. Ding, S. Cui, J. Lin, Z. Sun, P. Du, C. Chen, *Catal. Sci. Technol*. **2017**, *7*, 3056.

[5] F. Rieck genannt Best, J. Koch, G. Lilienkamp, F. Körkemeyer, H.J. Maier, J. Caro, K. Lange, *Int. J. Electrochem*. **2018,** *2018*, 9875438.

[6] J. Duan, S. Chen, C. Zhao, *Nat. Commun*. **2017**, *8*, 15341.

[7] C. Xiao, Y. Li, X. Lu, C. Zhao, *Adv. Funct. Mater*. **2016**, *26*, 3515.

[8] D. Senthil Raja, H.W. Lin, S.Y. Lu, *Nano Energy*, **2019**, *57*, 1.

[9] Z. Chen, H. Xu, Y. Ha, X. Li, M. Liu, R. Wu, *Appl. Catal. B Environ*. **2019**, *250*, 213.

[10] D. Zhong, L. Zhang, C. Li, D. Li, C. Wei, Q. Zhao, J. Li, J. Gong, *J. Mater. Chem. A*. **2018**, *6*, 16810.

[11] J. Wang, L. Ji, Z. Chen, *ACS Catal*. **2016**, *6* (2016) 6987.

[12] B.H.R. Suryanto, Y. Wang, R.K. Hocking, W. Adamson, C. Zhao, *Nat. Commun*. **2019**, *10*, 5599.

[13] M. Yu, Z. Wang, J. Liu, F. Sun, P. Yang, J. Qiu, *Nano Energy*, **2019**, *63*, 103880.

[14] S.H. Ahn, A. Manthiram, *Small*, **2020**, *16*, 2002511.

[15] Z.-X. Shi, J.-W. Zhao, C.-F. Li, H. Xu, G.-R. Li, *Appl. Catal. B Environ*, **2021**, *298*, 120558.

[16] M. Qu, Y. Jiang, M. Yang, S. Liu, Q. Guo, W. Shen, M. Li, R. He, *Appl. Catal. B Environ*, **2020***, 263*, 118324.